NASA/TM-2008-215314

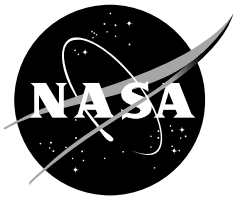

Modeling the Non-Linear Response of Fiber-Reinforced Laminates Using a Combined Damage/Plasticity Model

Clara Schuecker
NASA Postdoctoral Program at NASA Langley Research Center, Hampton, Virginia

Carlos G. Dávila
NASA Langley Research Center, Hampton, Virginia

Heinz E. Pettermann
Vienna University of Technology, Vienna, Austria

July 2008

The NASA STI Program Office ... in Profile

Since its founding, NASA has been dedicated to the advancement of aeronautics and space science. The NASA Scientific and Technical Information (STI) Program Office plays a key part in helping NASA maintain this important role.

The NASA STI Program Office is operated by Langley Research Center, the lead center for NASA's scientific and technical information. The NASA STI Program Office provides access to the NASA STI Database, the largest collection of aeronautical and space science STI in the world. The Program Office is also NASA's institutional mechanism for disseminating the results of its research and development activities. These results are published by NASA in the NASA STI Report Series, which includes the following report types:

- TECHNICAL PUBLICATION. Reports of completed research or a major significant phase of research that present the results of NASA programs and include extensive data or theoretical analysis. Includes compilations of significant scientific and technical data and information deemed to be of continuing reference value. NASA counterpart of peer-reviewed formal professional papers, but having less stringent limitations on manuscript length and extent of graphic presentations.

- TECHNICAL MEMORANDUM. Scientific and technical findings that are preliminary or of specialized interest, e.g., quick release reports, working papers, and bibliographies that contain minimal annotation. Does not contain extensive analysis.

- CONTRACTOR REPORT. Scientific and technical findings by NASA-sponsored contractors and grantees.

- CONFERENCE PUBLICATION. Collected papers from scientific and technical conferences, symposia, seminars, or other meetings sponsored or co-sponsored by NASA.

- SPECIAL PUBLICATION. Scientific, technical, or historical information from NASA programs, projects, and missions, often concerned with subjects having substantial public interest.

- TECHNICAL TRANSLATION. English-language translations of foreign scientific and technical material pertinent to NASA's mission.

Specialized services that complement the STI Program Office's diverse offerings include creating custom thesauri, building customized databases, organizing and publishing research results ... even providing videos.

For more information about the NASA STI Program Office, see the following:

- Access the NASA STI Program Home Page at ***http://www.sti.nasa.gov***

- E-mail your question via the Internet to help@sti.nasa.gov

- Fax your question to the NASA STI Help Desk at (301) 621-0134

- Telephone the NASA STI Help Desk at (301) 621-0390

- Write to:
  NASA STI Help Desk
  NASA Center for AeroSpace Information
  7115 Standard Drive
  Hanover, MD 21076-1320

NASA/TM-2008-215314

Modeling the Non-Linear Response of Fiber-Reinforced Laminates Using a Combined Damage/Plasticity Model

Clara Schuecker
NASA Postdoctoral Program at NASA Langley Research Center, Hampton, Virginia

Carlos G. Dávila
NASA Langley Research Center, Hampton, Virginia

Heinz E. Pettermann
Vienna University of Technology, Vienna, Austria

National Aeronautics and
Space Administration

NASA Langley Research Center
Hampton, VA 23681

July 2008

Available from:

NASA Center for AeroSpace Information (CASI)
7115 Standard Drive
Hanover, MD 21076-1320
(301) 621-0390

National Technical Information Service (NTIS)
5285 Port Royal Road
Springfield, VA 22161-2171
(703) 605-6000

Modeling the non-linear response of fiber-reinforced laminates using a combined damage/plasticity model

C. Schuecker[1], C. G. Dávila[2], and H. E. Pettermann[3]

[1] *NASA Postdoctoral Program*
at *NASA Langley Research Center, Hampton, VA 23681*

[2] *Durability, Damage Tolerance, and Reliability Branch*
NASA Langley Research Center, Hampton, VA 23681

[3] *Austrian Aeronautics Research (AAR) / Network for Materials and Engineering*
at the *Institute of Lightweight Design and Structural Biomechanics,*
Vienna University of Technology, Gusshausstr. 27-29/E317, 1040 Vienna, Austria

Abstract

The present work is concerned with modeling the non-linear response of fiber reinforced polymer laminates. Recent experimental data suggests that the non-linearity is not only caused by matrix cracking but also by matrix plasticity due to shear stresses. To capture the effects of those two mechanisms, a model combining a plasticity formulation with continuum damage has been developed to simulate the non-linear response of laminates under plane stress states. The model is used to compare the predicted behavior of various laminate lay-ups to experimental data from the literature by looking at the degradation of axial modulus and Poisson's ratio of the laminates. The influence of residual curing stresses and in-situ effect on the predicted response is also investigated.

It is shown that predictions of the combined damage / plasticity model, in general, correlate well with the experimental data. The test data shows that there are two different mechanisms that can have opposite effects on the degradation of the laminate Poisson's ratio which is captured correctly by the damage / plasticity model. Residual curing stresses are found to have a minor influence on the predicted response for the cases considered here. Some open questions remain regarding the prediction of damage onset.

Key words: Fiber Reinforced Laminates, Polymer Matrix Composites, Computational Mechanics, Non-Linear Material Response, Continuum Damage, Plasticity, Puck Failure Criterion.

Notation

Indices:

$\mathsf{1}, \mathsf{2}, \mathsf{3}$	...	ply coordinates ($\mathsf{1}$ – fiber, $\mathsf{2}$ – transverse in-plane, $\mathsf{3}$ – out-of-plane direction)
$\mathsf{l}, \mathsf{n}, \mathsf{t}$	...	fracture plane coordinates (l – fiber, n – normal, t – transverse direction)
x, y	...	global coordinates (x – loading direction, y – transverse to load, in plane)

Roman letters:

$\boldsymbol{C}^{\mathrm{d}}$	...	compliance tensor of damaged ply
$\boldsymbol{C}^{\mathrm{init}}$	...	compliance tensor of initial (undamaged) ply
$\boldsymbol{E}^{\mathrm{d}}$	...	elasticity tensor of damaged ply
$\boldsymbol{E}^{\mathrm{incl}}$	...	elasticity tensor of inclusions in Mori-Tanaka formulation
$\boldsymbol{E}^{\mathrm{init}}$	...	elasticity tensor of initial (undamaged) ply
E_i	...	Young's modulus in i-direction
e_{n}	...	inclusion aspect ratio normal to fracture plane
f_{E}	...	factor of effort
$G_{\mathrm{Ic,ply}}$	...	critical energy release rate for intra-ply cracking in mode I
$G^{\mathrm{Th}}_{\mathrm{Ic,ply}}$	...	critical energy release rate for intra-ply cracking in mode I including residual stresses
$G_{\mathrm{IIc,ply}}$	...	critical energy release rate for intra-ply cracking in mode II
$G^{\mathrm{Th}}_{\mathrm{IIc,ply}}$	...	critical energy release rate for intra-ply cracking in mode II including residual stresses
G_{ij}	...	shear modulus for ij-shear deformation
$G^{\mathrm{incl}}_{\mathsf{nl}} = G^{\mathrm{incl}}_{\mathsf{nt}}$	...	inclusion shear modulus in the fracture plane
$\boldsymbol{I}$	...	fourth order identity matrix
k	...	parameter of shear plasticity law
n	...	exponent of shear plasticity law
p^{t}_{12}, p^{c}_{12}	...	slope parameters for Puck failure criterion
$\boldsymbol{S}$	...	Eshelby tensor
S	...	nominal shear strength
S_{is}	...	in-situ shear strength of a ply cluster in a laminate
t	...	thickness of a cluster of equally oriented plies
t^{ply}	...	thickness of one single ply
Y	...	nominal transverse tensile strength
$Y^{\mathrm{t}}_{\mathrm{is}}$	...	in-situ transverse tensile strength of a ply cluster in a laminate

Greek letters:

β	...	lay-up angle of off-axis plies
γ_{ij}	...	engineering shear strain on plane i in direction j
$\gamma_{\mathrm{is}}^{\mathrm{ult}}$	...	shear strain under in-plane simple shear at failure ($\sigma_{12} = S_{\mathrm{is}}$)
$\gamma_{\mathtt{n}i}^{\mathrm{pl}}$	...	plastic shear strain component in the fracture plane in direction i
$\gamma_{\mathtt{n}\psi}^{\mathrm{pl}}$	...	magnitude of plastic shear strain in the fracture plane
$\boldsymbol{\varepsilon}$	...	strain tensor
$\boldsymbol{\varepsilon}^{\mathrm{pl}}$	...	plastic strain tensor
ε_{ii}	...	normal strain component on plane i in direction i
κ	...	damage evolution parameter
μ_{D}	...	damage parameter for shear stiffness recovery under compression
$\mu_{\mathtt{n}\psi}^{\mathrm{pl}}$	...	parameter for influence of normal stress on shear plasticity
μ_{12}^{pl}	...	influence parameter under in-plane simple shear, σ_{12}
μ_{23}^{pl}	...	influence parameter under out-of-plane simple shear, σ_{23}
ν_{21}	...	minor in-plane Poisson's ratio ($\nu_{21} = \nu_{12}\, E_2/E_1$)
ψ	...	angle between $\mathtt{t}$-coordinate and fracture plane shear stress vector
$\vec{\boldsymbol{\sigma}}_{\mathrm{fp}}$	...	traction vector of the fracture plane
$\boldsymbol{\sigma}$	...	ply stress tensor
$\boldsymbol{\sigma}^{\mathrm{FPF}}$	...	ply stress tensor at failure (i.e. when ply failure criterion is fulfilled)
σ_{ij}	...	stress component on plane i in direction j
$\sigma_{\mathtt{n}\mathtt{i}}$	...	shear stress component on the fracture plane in direction i
$\sigma_{\mathtt{n}\psi}$	...	total shear stress on fracture plane (projection of traction vector)
$\sigma_{\mathtt{n}\psi}^{\mathrm{eq}}$	...	equivalent fracture plane stress
θ_{fp}	...	fracture plane angle predicted by Puck failure criterion
ξ	...	damage state variable
ξ^{sat}	...	damage state variable at saturation

1 INTRODUCTION

The use of fiber reinforced polymer (FRP) composites is increasingly popular in industries where lightweight design is beneficial. In order to achieve further weight reductions without compromising the reliability of composite parts, accurate prediction of the material response is essential. Due to their complex, hierarchical micro-structure, the load response of laminated composites is influenced by a number of physical mechanisms. Ultimate failure of laminates is typically caused by fiber failure or delamination. Prior to failure, plastic deformation and cracking of the weaker matrix constituent may lead to non-linearity and can influence other failure modes through load redistribution and by creating local stress concentrations.

Although matrix failure normally does not lead to ultimate laminate failure directly, the modeling of non-linearities caused by the matrix is important for two reasons. On the one hand, accurate modeling of load redistribution is necessary with respect to the influence of the matrix response on other failure modes such as fiber failure or delamination. On the other hand, the serviceability of a structure may be determined by criteria other than strength that depend on the matrix response, for example, if a maximum allowable deformation requirement has to be met or if matrix cracks cannot be tolerated (e.g. in pressure vessels). Consequently, the mechanisms of matrix-dominated behavior of laminates need to be understood and their effects captured appropriately by laminate models in order to improve predictions of the load response and failure of laminates.

The modeling of non-linearities caused by the matrix has been very much focused on continuum damage mechanics [12, 21] where it is assumed that an accumulation of brittle matrix cracks is responsible for the observed non-linearity. Rather than looking at discrete cracks, however, continuum damage models simulate the response of a cracked ply by modifying the elastic properties of the homogenized ply depending on some internal state variables. A number of continuum damage models for stiffness degradation due to matrix cracking under plane stress states have been presented in the literature [1, 2, 4, 7, 11, 20, 24, 26, 28]. These models have proven to be successful in predicting the non-linear response when the damaged plies experience primarily tensile stresses perpendicular to the fiber direction. Under shear-dominated loading, however, comparisons between model predictions and experimental data have been less satisfactory. Recent research suggests that the non-linear response under shear dominated ply loads cannot be attributed to brittle mechanisms alone [16, 30, 31].

To model the non-linear response of composite plies under shear-dominated loading, a plasticity model has recently been proposed [25] and combined with

a damage model developed previously [22, 24, 26]. It is implemented with an extended version of classical lamination theory (CLT) to provide for analysis of multi-axial laminates under plane stress states including thermal and moisture effects. The combined damage / plasticity model provides significant improvements over the original brittle damage model as shown by comparing predictions of the two models to experimental data [25]. In addition to providing better correlation with experimental data, the combined model captures the non-linear response of uni-directional (UD) laminates as well as residual strains after unloading, and it is able to explain discrepancies between the shear response that can be observed when using different test methods.

In the present paper, the combined damage / plasticity model is used to investigate effects of in-situ strength and residual stresses on the non-linear load response of laminates. First, the formulation of the combined model is briefly reviewed. Next, the influence of non-linear shear behavior on the predicted in-situ strength following a method proposed by Camanho *et al.* [6] is discussed. Predictions of the combined model are finally compared to two series of experimental tests by Varna *et al.* [31, 32].

2 COMBINED DAMAGE / PLASTICITY MODEL

The combined damage / plasticity model assumes that damage occurs in the form of brittle matrix cracks that span the whole thickness of a ply and lead to a degradation of the homogenized ply stiffness. Damage can only develop in plies embedded in a multi-axial laminate because the first matrix crack in a UD laminate corresponds to ultimate failure. Consequently, any non-linearity prior to damage onset in embedded plies and all non-linearity in UD laminates is attributed to plasticity. The constitutive equation of the combined model that relates the ply stress tensor, $\boldsymbol{\sigma}$, to the ply strain tensor, $\boldsymbol{\varepsilon}$, is given by

$$\boldsymbol{\sigma} = \boldsymbol{E}^{\mathrm{d}} \left(\boldsymbol{\varepsilon} - \boldsymbol{\varepsilon}^{\mathrm{pl}} \right) \quad , \tag{1}$$

where $\boldsymbol{\varepsilon}^{\mathrm{pl}}$ is the plastic strain tensor defined by the plasticity model and $\boldsymbol{E}^{\mathrm{d}}$ is the elasticity tensor of a damaged ply given by the damage model. Both of these tensors can contribute to the non-linear response.

The damage and plasticity formulations used herein are based on the Puck failure hypothesis for matrix dominated failure in fiber reinforced composites [17, 20, 23]. According to Puck, fracture occurs in a plane that is parallel to the fiber orientation and defined by a fracture plane angle, θ_{fp}, as depicted in Fig. 1, left. For plane stress states, the fracture plane is perpendicular to the laminate plane ($\theta_{\mathrm{fp}} = 0$) under combinations of transverse tensile stresses and in-plane shear or moderate transverse compression and in-plane shear. For

high transverse compression combined with shear, the fracture plane angle is non-zero and can be computed analytically.

The Puck criterion for plane stress (Puck 2D) [17, 20, 23] is used in the damage model to predict the onset and evolution of damage under multi-axial stress states and to compute the fracture plane in which damage accumulates. In the plasticity model, the accumulation of plastic strain is also assumed to be associated with the fracture plane predicted by Puck 2D. This assumption is supported by recent experimental work showing shear bands in UD-laminates under uniaxial compression [3]. According to this study, the shear bands have the same orientation as ply cracks that develop when load is increased further, which suggests that the shear bands are precursors of ply cracks.

The damage/plasticity model is implemented in a stand-alone code combined with CLT to provide a tool for the non-linear analysis of multi-axial laminates. An extended version of CLT is used to allow for the consideration of plastic strains as well as the strains caused by moisture and thermal loads (e.g. [5]). The formulation of the damage and plasticity models is explained in the following sections.

2.1 Plasticity Formulation

The plasticity law assumes that plastic strains are caused by shear bands with the same orientation as the fracture plane predicted by Puck 2D. The plastic shear strain in that plane, $\gamma^{\mathrm{pl}}_{\mathsf{n}\psi}$, is related to the shear stress acting on the fracture plane, $\sigma_{\mathsf{n}\psi} = \sqrt{\sigma^2_{\mathsf{nl}} + \sigma^2_{\mathsf{nt}}}$, which is the projection of the traction vector, $\vec{\sigma}_{\mathrm{fp}}$, onto the fracture plane (see Fig. 1, right). The plastic shear strain is assumed to have the form

$$\gamma^{\mathrm{pl}}_{\mathsf{n}\psi} = \left(\frac{\sigma^{\mathrm{eq}}_{\mathsf{n}\psi}}{k} \right)^n \quad , \tag{2}$$

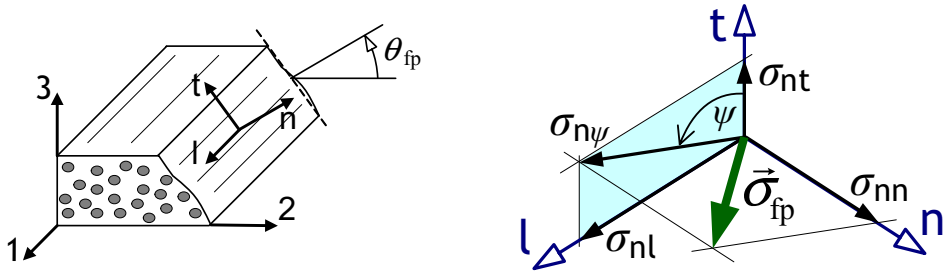

Fig. 1. Definition of fracture plane and corresponding coordinate system, l-n-t, with regard to the ply coordinate system, 1-2-3, by fracture plane angle, θ_{fp} (left); tractions on the fracture plane for $\theta_{\mathrm{fp}} \neq 0$ (right).

with plasticity parameters, k and n, and an equivalent stress, $\sigma^{\mathrm{eq}}_{\mathsf{n}\psi}$, defined as

$$\sigma^{\mathrm{eq}}_{\mathsf{n}\psi} = |\sigma_{\mathsf{n}\psi}| + \mu^{\mathrm{pl}}_{\mathsf{n}\psi}\sigma_{\mathsf{nn}} \quad , \tag{3}$$

to account for the influence of normal stress on the non-linear shear behavior that is observed in experiments [17, 19]. The factor $\mu^{\mathrm{pl}}_{\mathsf{n}\psi}$ is interpolated from the corresponding parameters for in-plane and out-of-plane shear, μ^{pl}_{12} and μ^{pl}_{23}, respectively, as

$$\mu^{\mathrm{pl}}_{\mathsf{n}\psi} = \mu^{\mathrm{pl}}_{12}\sin^2(\psi) + \mu^{\mathrm{pl}}_{23}\cos^2(\psi) \quad , \tag{4}$$

where ψ is the angle between the directions of σ_{nt} and $\sigma_{\mathsf{n}\psi}$ (cf. Fig. 1, right). The parameters μ^{pl}_{12} and μ^{pl}_{23} are considered to be material parameters that need to be derived from experimental data. In general, the two parameters are not the same due to the different effect of the ply micro-geometry in longitudinal and transverse direction resulting in a different influence of normal stresses on the longitudinal and transverse shear response. The parameter μ^{pl}_{23} can be determined from stress–strain data of a uni-axial transverse compression test on a UD-laminate. The factor μ^{pl}_{12} should be derived from experimental data of tests with varying stress ratio σ_{22}/σ_{12}. A detailed discussion of parameter identification for the plasticity model as well as a method for estimating μ^{pl}_{12} and μ^{pl}_{23} when the necessary experimental data is unavailable is given in [25].

Finally, splitting the plastic shear strain $\gamma^{\mathrm{pl}}_{\mathsf{n}\psi}$ into its two components, $\gamma^{\mathrm{pl}}_{\mathsf{nl}}$ and $\gamma^{\mathrm{pl}}_{\mathsf{nt}}$, and transformation to ply coordinates results in a strain tensor given by

$$\boldsymbol{\varepsilon}^{\mathrm{pl}} = \begin{cases} (0,0,0,\gamma^{\mathrm{pl}}_{12},0,0)^{\mathrm{T}} & \text{for} \quad \theta_{\mathrm{fp}} = 0 \\ (0,\varepsilon^{\mathrm{pl}}_{22},\varepsilon^{\mathrm{pl}}_{33},\gamma^{\mathrm{pl}}_{12},0,0)^{\mathrm{T}} & \text{for} \quad \theta_{\mathrm{fp}} \neq 0 \end{cases} \quad . \tag{5}$$

2.2 Damage Formulation

The elasticity tensor of a damaged ply, $\boldsymbol{E}^{\mathrm{d}}$, is predicted by a continuum damage model presented in [22, 24, 26]. In that model, a scalar damage state variable, ξ, is introduced as a measure for the amount of damage in a ply. This damage state variable can increase with load but can never decrease. The load acting on a ply is quantified by a factor of effort, f_{E}, which is determined from

$$\boldsymbol{\sigma}^{\mathrm{FPF}} f_{\mathrm{E}} = \boldsymbol{\sigma} \quad , \tag{6}$$

where $\boldsymbol{\sigma}$ is a given ply stress state and $\boldsymbol{\sigma}^{\mathrm{FPF}}$ is the corresponding failure stress state determined from the Puck 2D failure criterion. The damage state variable is related to the factor of effort by a damage evolution law of the form

$$\frac{\xi}{\xi^{\mathrm{sat}}} = \begin{cases} 0 & \text{for} \quad f_{\mathrm{E}} \leq \frac{1}{1+\kappa} \\ 1 - \exp\left(-\frac{(f_{\mathrm{E}}(1+\kappa)-1)^2}{2\kappa^2}\right) & \text{for} \quad f_{\mathrm{E}} \geq \frac{1}{1+\kappa} \end{cases} \quad , \tag{7}$$

with one damage evolution parameter κ. The maximum amount of damage that can be reached in a ply is given by the damage state variable at saturation, ξ^{sat}. The general shape of the evolution law function is chosen based on experimental observations regarding the increasing crack density with load (e.g. [14, 20]). In terms of continuum damage modeling, the development of cracks is equivalent to an increase of the damage state variable, ξ. According to the evolution law in Eq. 7, damage starts to develop when $f_{\mathrm{E}} = \frac{1}{1+\kappa}$ is fulfilled. The evolution parameter κ, therefore, determines the damage onset load and controls how quickly damage progresses with an increase of load. For example, the evolution law converges to the step function for $\kappa = 0$ such that damage onset occurs at $f_{\mathrm{E}} = 1$ and the final damage state ξ^{sat} is reached instantly.

The effect of a given damage state on the elastic response of a ply is predicted by the Mori-Tanaka method [13]. By this approach, the elasticity tensor of a material containing aligned ellipsoidal inclusions is computed as a function of the inclusion aspect ratio, e_{n}, and the elastic properties of the inclusions and the surrounding material. In the damage model, the Mori-Tanaka method is employed using penny-shaped inclusions that are aligned with the fracture plane predicted by Puck 2D. Note that these inclusions are not intended to represent actual cracks in the material, rather they are used to derive the anisotropic elasticity tensor of the damaged material in a thermodynamically consistent way. Based on the formulation of Tandon and Weng [29], the compliance tensor of the damaged material as a function of ξ is given by

$$\begin{aligned}&\boldsymbol{C}^{\mathrm{d}} = \left(\boldsymbol{E}^{\mathrm{d}}\right)^{-1} = \\ &\left\{\boldsymbol{I} - \xi\left[(\boldsymbol{E}^{\mathrm{incl}} - \boldsymbol{E}^{\mathrm{init}}) : (\boldsymbol{S} - \xi(\boldsymbol{S} - \boldsymbol{I})) + \boldsymbol{E}^{\mathrm{init}}\right]^{-1} : \left[\boldsymbol{E}^{\mathrm{incl}} - \boldsymbol{E}^{\mathrm{init}}\right]\right\} : \boldsymbol{C}^{\mathrm{init}} \quad ,\end{aligned} \tag{8}$$

where $\boldsymbol{E}^{\mathrm{incl}}$ denotes the elasticity tensor of the fictitious inclusions, $\boldsymbol{E}^{\mathrm{init}}$ and $\boldsymbol{C}^{\mathrm{init}}$ are the elasticity and compliance tensors of the initial (undamaged) material, respectively, $\boldsymbol{S}$ is the Eshelby tensor, and $\boldsymbol{I}$ is the 4^{th} order identity matrix. The elastic properties assigned to the inclusions depend on the stress state. If the normal stress on the corresponding fracture plane, σ_{nn}, is tensile such that cracks would be open, the inclusions become voids with zero stiffness ($\boldsymbol{E}^{\mathrm{incl}} = \boldsymbol{0}$). For compressive normal stress, the properties of the inclusions are defined to be the same as those of the initial (undamaged) ply material except for reduced shear moduli in the fracture plane, $G^{\mathrm{incl}}_{\mathsf{nl}}$ and $G^{\mathrm{incl}}_{\mathsf{nt}}$, which are computed as

$$G^{\mathrm{incl}}_{\mathsf{nl}} = G^{\mathrm{incl}}_{\mathsf{nt}} = \mu_{\mathrm{D}}|\sigma_{\mathsf{nn}}| \quad , \tag{9}$$

where the factor μ_{D} is a material parameter accounting for shear stiffness recovery due to friction at the crack faces.

In order to fully define the damage model, the four parameters κ, ξ^{sat}, e_{n}, and μ_{D} need to be defined. Damage typically progresses very quickly with increasing load. Reasonable values for the evolution parameter are therefore in the range of $\kappa = 0.01 - 0.05$, which means that damage onset in the model occurs at $99\% - 95\%$ of the nominal failure load. The saturation state is normally set to $\xi^{\mathrm{sat}} = 0.2$ for lack of better information and because the Mori-Tanaka approach becomes increasingly inaccurate for $\xi > 0.2$. It should be noted, however, that the choice of ξ^{sat} is not particularly relevant because final failure, e.g. due to fiber failure, is typically reached before crack saturation occurs. The inclusion aspect ratio normal to the fracture plane, e_{n}, which enters into the computation of the Eshelby tensor, is chosen to be very small such as to resemble a crack-like geometry. As long as $e_{\mathsf{n}} < 0.01$, the exact choice of e_{n} has little effect on the damage model predictions. Little is known about the correct choice of μ_{D}. A value in the range of $\mu_{\mathrm{D}} = 10 - 15$ has previously yielded good results, however, a conservative approach would be to assume no shear stiffness recovery between the crack faces and setting $\mu_{\mathrm{D}} = 0$.

2.3 In-situ strength with non-linear shear behavior

It has been found in experiments that the transverse tensile and shear strengths of a ply embedded in a multi-axial laminate are higher than those of a unidirectional (UD) material (e.g. [8, 15]). This effect is commonly termed 'in-situ' effect. It increases with decreasing thickness of a ply (or the number of equally oriented plies clustered together) and also depends on the location of a ply in the laminate (inner or outer ply). In the damage model, the in-situ effect can be taken into account by employing in-situ strengths, $Y_{\mathrm{is}}^{\mathrm{t}}$ and S_{is}, rather than UD laminate strengths in the Puck 2D criterion which is used in the model to determine damage onset under multi-axial stress states.

For the current work, an analytical solution proposed by Camanho *et al.* [6] is used to compute in-situ strengths. The in-situ solution for thin embedded plies assumes an initial flaw in the form of a crack whose size is equal to the thickness of a ply or cluster of equally oriented plies, t. The in-situ strength is assumed to correspond to the uni-axial stress at which this initial crack would start to grow parallel to the fiber direction. The start of crack growth is determined based on fracture mechanics. For transverse tension, the approach gives the in-situ strength as

$$\begin{aligned} Y_{\mathrm{is}}^{\mathrm{t}} &= \sqrt{\frac{4G_{\mathrm{Ic,ply}}}{\pi a_0 \Lambda_{22}^0}} \\ \text{with} \quad \Lambda_{22}^0 = 2\left(\frac{1}{E_2} - \frac{\nu_{21}^2}{E_1}\right) \quad &\text{and} \quad a_0 = \begin{cases} t/2 & \dots \text{inner ply} \\ t & \dots \text{outer ply} \end{cases} , \end{aligned} \tag{10}$$

where $G_{\mathrm{Ic,ply}}$ is the critical energy release rate for mode I intra-laminar crack propagation in the fiber direction, and E_1, E_2, and $\nu_{21} = \nu_{12}E_2/E_1$ are the ply's longitudinal and transverse Young's moduli and minor Poisson's ratio.

The in-situ shear strength has to take the non-linear shear response into account and is determined following Ref. [6] from

$$2\int_0^{\gamma_{\mathrm{is}}^{\mathrm{ult}}} \sigma_{12}(\gamma_{12})\,\mathrm{d}\gamma_{12} = \frac{4G_{\mathrm{IIc,ply}}}{\pi a_0} \quad \text{with} \quad a_0 = \begin{cases} t/2 & \ldots \text{inner ply} \\ t & \ldots \text{outer ply} \end{cases} \quad , \tag{11}$$

where $G_{\mathrm{IIc,ply}}$ denotes the mode II critical energy release rate associated with intra-laminar crack propagation parallel to the fiber direction, and $\gamma_{\mathrm{is}}^{\mathrm{ult}}$ refers to the shear strain at the crack propagation load that corresponds to $\sigma_{12} = S_{\mathrm{is}}$. The non-linear relation for in-plane simple shear given by the plasticity model (prior to damage onset) is determined from Eq. 2 for $\sigma_{\mathrm{n}\psi}^{\mathrm{eq}} = \sigma_{12}$ as

$$\gamma_{12} = \gamma_{12}^{\mathrm{el}} + \gamma_{12}^{\mathrm{pl}} = \frac{\sigma_{12}}{G_{12}} + \left(\frac{\sigma_{12}}{k}\right)^n \quad . \tag{12}$$

From Eq. 12, it follows that

$$\mathrm{d}\gamma_{12} = \left(\frac{1}{G_{12}} + \frac{n}{k^n}\left(\frac{\sigma_{12}}{k}\right)^{n-1}\right)\mathrm{d}\sigma_{12} \quad . \tag{13}$$

Using Eq. 13 in the integral on the left hand side of Eq. 11 leads to

$$\frac{1}{2G_{12}}\,S_{\mathrm{is}}^2 + \frac{n}{(n+1)k^n}\,S_{\mathrm{is}}^{n+1} = \frac{2G_{\mathrm{IIc,ply}}}{\pi a_0} \quad . \tag{14}$$

The in-situ shear strength, S_{is}, is given by the real positive root of Eq. 14. If the exponent n is an odd positive integer, a closed form solution can be obtained for Eq. 14 which, in that case, has exactly one real positive root. Hahn and Tsai [9] proposed to use a third order polynomial to approximate the non-linear shear response. It has been found, however, that a higher exponent typically yields a better description of the non-linear shear response [25]. It is therefore suggested here to choose an exponent of $n = 5$ or $n = 7$.

3 COMPARISON TO EXPERIMENTAL DATA

The combined damage / plasticity model is used to simulate the load response of glass fiber / epoxy laminates with varying lay-up under uniaxial tension. Predictions for the degradation of axial modulus and Poisson's ratio as functions of axial strain are compared to experimental data by Varna *et al.* [10, 31, 32].

Table 1
Material data of the glass fiber / epoxy material [10, 31, 32] and parameters used in the damage / plasticity model.

Elastic and thermal properties					
E_1	E_2	G_{12}	ν_{12}	ΔT	$\alpha_2 - \alpha_1$
[GPa]	[GPa]	[GPa]		[K]	[1/K]
44.73	12.8	5.8	0.3	-120	1 E-5

Plasticity and damage parameters					
n	k	μ_{12}^{pl}	κ	e_{n}	ξ^{sat}
7	147.1 MPa	0	0.05	0.001	0.2

3.1 Model Parameters for the Glass Fiber / Epoxy Material tested

The material used in the experiments is a toughened glass fiber / epoxy system (material specifications are not given in the references). The determination of model parameters for the material system is discussed in this section. The ply properties and model parameters used in the analyses are summarized in Table 1. Elastic and thermal properties are taken from [31] with ΔT referring to the assumed temperature change from a stress free state to ambient temperature and $\alpha_2 - \alpha_1$ denoting the difference between the coefficients of thermal expansion in longitudinal and transverse directions.

Parameters for the plasticity formulation (Sec. 2.1) are determined from the non-linear shear response derived from tensile tests on angle ply laminates, $(\pm\beta_4)_{\mathrm{s}}$, with two different lay-up angles $\beta = 27°$ and $\beta = 40°$ [31]. The experimental data is shown in Fig. 2, left, including the analytical curve fit for $n = 7$ and $k = 147.1\,\mathrm{MPa}$. The two lay-up angles lead to different stress ratios of $\sigma_{22}/\sigma_{12} = -0.06$ for $\beta = 27°$ and $\sigma_{22}/\sigma_{12} = 0.3$ for $\beta = 40°$. Since there is little difference between the data from these two laminates, it is assumed that the shear response is independent of transverse normal stresses, and the influence parameter for in-plane shear, μ_{12}^{pl}, is set to zero. The parameter μ_{23}^{pl} is not relevant for the test cases shown here since the predicted fracture plane angle is always zero, resulting in $\psi = 90°$ for plane stress states (see Eq. 4 and Fig. 1).

For the damage model (Sec. 2.2), the damage evolution parameter is chosen as $\kappa = 0.05$, which leads to a quick progression of damage as is typically observed in experiments, and the inclusion aspect ratio is selected to be very small, $e_{\mathsf{n}} = 0.001$, to resemble crack like voids. The damage variable at saturation

is set to $\xi^{\mathrm{sat}} = 0.2$, however, this parameter is found to have no influence on the results presented since saturation is not reached within the strain range considered.

The degradation of elastic ply properties resulting from the chosen set of damage parameters is shown in Fig. 2, right, for the 90° ply of a $(0_2/90_4)_\mathrm{s}$ laminate under uniaxial tension. Damage onset occurs at 95% of the predicted ply failure load as a result of $\kappa = 0.05$. For a smaller value of κ, damage onset in Fig. 2, right, would shift to slightly higher strains (at most, to $\varepsilon_{22} = 0.6\%$ for $\kappa = 0$). The different degradation of elastic properties in the model is controlled by the inclusion aspect ratio e_n. For a spherical inclusion ($e_\mathsf{n} = 1$), all four degradation curves would coincide. For the thin, crack-like voids used in the damage model, there is almost no change of E_1 and ν_{12}, a pronounced reduction of E_2, and less severe degradation of G_{12} (Fig. 2, right). This characteristic is consistent with analytical solutions for the stiffness degradation of a cracked ply (e.g. [7]).

Ply strength values and critical energy release rates for the glass fiber composite are not given in [10, 31, 32]. The mode I critical energy release rate can be back-computed from data of the $(0_2/90_4)_\mathrm{s}$ laminate test. According to [10], cracking of the 90° layers for the $(0_2/90_4)_\mathrm{s}$ layup starts at approximately $\varepsilon_{xx} = 0.6\%$ (where x denotes the loading direction and y is the in-plane transverse direction). If curing stresses are disregarded, this strain state corresponds to a transverse stress in the 90° plies computed via CLT of $\sigma_{22} = 76\,\mathrm{MPa}$. Assuming that this value represents the in-situ transverse tensile strength, $Y^{\mathrm{t}}_{\mathrm{is}}$, of an 8-ply cluster with $t^{\mathrm{ply}} = 0.144\,\mathrm{mm}$, the mode I critical energy release rate can be computed by inverting Eq. 10 with $a_0 = 8\,t^{\mathrm{ply}}/2 = 0.576\,\mathrm{mm}$ as $G_{\mathrm{Ic,ply}} = 0.4\,\mathrm{kJ/m^2}$. This value lies on the upper end of the typical range of

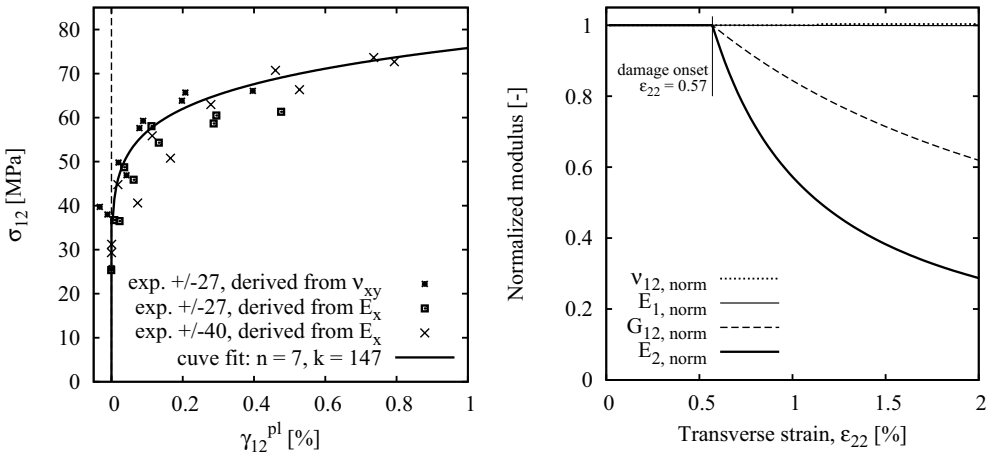

Fig. 2. Non-linear shear response from experimental data of two different laminate tests by Varna *et al.* [31] and analytical curve fit for the plasticity formulation (left); degradation of elastic ply properties predicted by the damage model (right).

Table 2
Critical energy release rates and Puck 2D slope parameters used in the analyses.

$G_{\mathrm{Ic,ply}}$	$G_{\mathrm{IIc,ply}}$	$G^{\mathrm{Th}}_{\mathrm{Ic,ply}}$	$G^{\mathrm{Th}}_{\mathrm{IIc,ply}}$	p^{t}_{12}	p^{c}_{12}
$[\mathrm{kJ/m^2}]$	$[\mathrm{kJ/m^2}]$	$[\mathrm{kJ/m^2}]$	$[\mathrm{kJ/m^2}]$		
0.4	0.8	0.51	1.02	0.3	0.25

energy release rates determined by standard tests for mode I fracture. If the same procedure is followed including curing stresses in the CLT equation by assuming a thermal load $\Delta T = -120\,\mathrm{K}$, a failure strain of $\varepsilon_{\mathrm{xx}} = 0.6\%$ corresponds to transverse stresses $\sigma_{22} = 85\,\mathrm{MPa}$ which leads to $G^{\mathrm{Th}}_{\mathrm{Ic,ply}} = 0.51\,\mathrm{kJ/m^2}$ following Eq. 10.

Since there is no experimental data available regarding shear failure, the mode II critical energy release rate is estimated as $G_{\mathrm{IIc,ply}} = 2\,G_{\mathrm{Ic,ply}}$ which corresponds to the typical $G_{\mathrm{IIc,ply}}/G_{\mathrm{Ic,ply}}$ ratio for ply fracture for several carbon fiber / epoxy composites given in [27]. The values of $G_{\mathrm{IIc,ply}}$ and $G^{\mathrm{Th}}_{\mathrm{IIc,ply}}$ lead to 8-ply in-situ shear strengths of $S_{\mathrm{is}} = 72.2\,\mathrm{MPa}$ and $S^{\mathrm{Th}}_{\mathrm{is}} = 73.5\,\mathrm{MPa}$, respectively, which are consistent with typical values for glass fiber / epoxy. It is clear that these values are only a rough estimate and a variation of $G_{\mathrm{IIc,ply}}$ will influence the predicted damage onset in plies that are loaded mainly by shear stresses. For the examples shown here, a higher value of $G_{\mathrm{IIc,ply}}$ would shift damage onset in off-axis plies to higher strains. However, the non-linearity under shear loading is dominated by plasticity rather than damage and the effect is therefore not very significant.

Finally, the slope parameters for the Puck 2D criterion, p^{t}_{12} and p^{c}_{12}, are chosen as $p^{\mathrm{t}}_{12} = 0.3$ and $p^{\mathrm{c}}_{12} = 0.25$ which correspond to the values suggested by Puck for glass fiber / epoxy materials [18]. Strength data for fiber failure and compressive failure is not relevant for the test cases considered here. The parameters related to ply strength predictions are summarized in Table 2.

3.2 Laminate tests $(\pm\beta/90_4)_s$

The first series of tested laminates has a lay-up of $(\pm\beta/90_4)_{\mathrm{s}}$ with four different angles $\beta = 0°, 15°, 30°, 40°$. Three analyses are performed for each of the laminates and compared to experimental data [32] as shown in Figs. 3–6. In a first analysis, the in-situ effect is not taken into account and 8-ply strengths without residual stresses are used for all layers (i.e. $Y^{\mathrm{t}} = 76\,\mathrm{MPa}$ and $S = 72.2\,\mathrm{MPa}$). The corresponding curves in Figs. 3–6 are labeled as 'nominal'. The other two analyses use in-situ strengths computed from Eqs. 10 and 11 based on the thickness of each ply cluster and its location (inner

or outer). The curves denoted by 'in-situ' are computed without residual stresses ($G_{\mathrm{Ic,ply}} = 0.4\,\mathrm{kJ/m^2}$, $G_{\mathrm{IIc,ply}} = 0.8\,\mathrm{kJ/m^2}$), while the analyses for curves '$\Delta T = -120\,\mathrm{K}$' include the effect of residual stresses by a superimposed thermal load and using $G^{\mathrm{Th}}_{\mathrm{Ic,ply}} = 0.51\,\mathrm{kJ/m^2}$ and $G^{\mathrm{Th}}_{\mathrm{IIc,ply}} = 1.02\,\mathrm{kJ/m^2}$. The strength values used in the three analyses are summarized in Table 3.

The degradation in Figs. 3–6 is caused primarily by transverse cracking in the 90° plies. In fact, Varna *et al.* [32] assumed that cracking occurs only in those layers. For the $(0_2/90_4)_\mathrm{s}$ laminate (Fig. 3), all three analyses yield exactly the same result since below 2% axial strain the 0° plies do not develop any matrix cracking and the predicted response of 90° plies is the same for all three analyses.

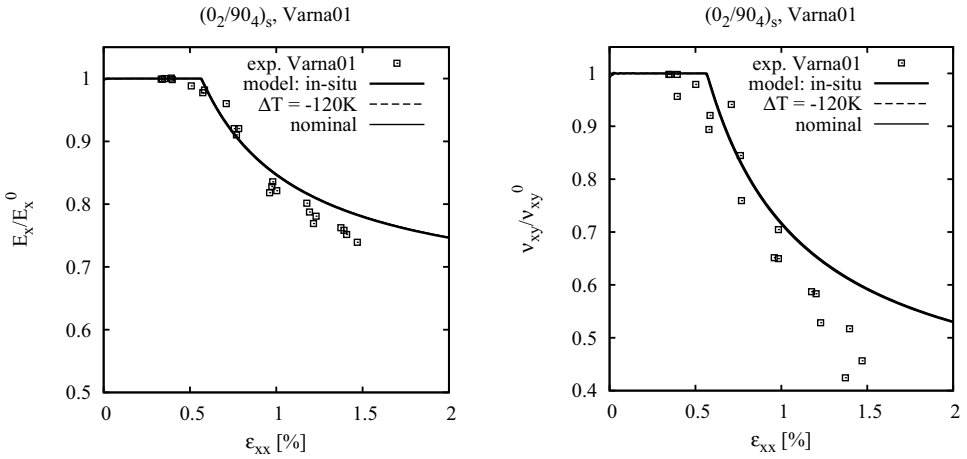

Fig. 3. Results for lay-up $(0_2/90_4)_\mathrm{s}$; axial modulus (left) and laminate Poisson's ratio (right) normalized by their initial value; experimental data from [32].

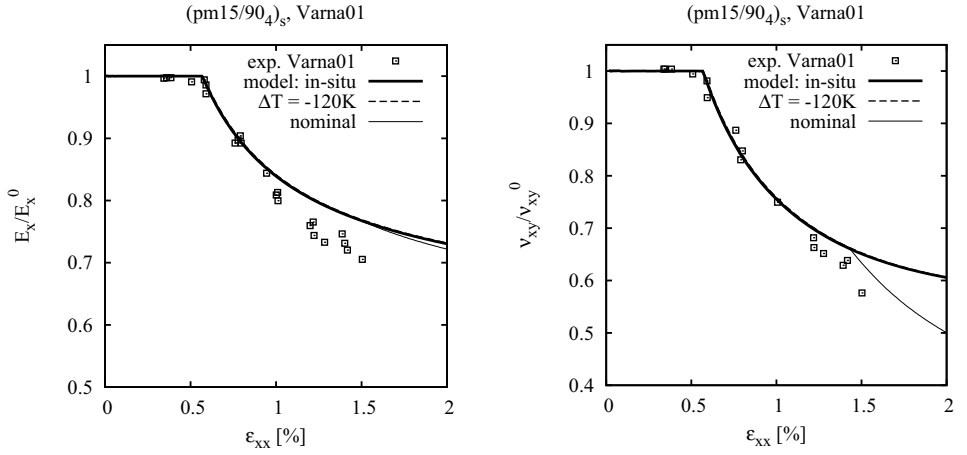

Fig. 4. Results for lay-up $(\pm 15/90_4)_\mathrm{s}$; axial modulus (left) and laminate Poisson's ratio (right) normalized by their initial value; experimental data from [32].

For the $(\pm 15/90_4)_s$ laminate (Fig. 4), the 'nominal' analysis predicts damage onset in the angle plies at approximately $\varepsilon_{xx} = 1.5\%$ in addition to damage of the 90° plies. This leads to a kink in the degradation curve of Poisson's ratio while the effect on Young's modulus degradation is only minimal. Similar observations can be made for the 'nominal' predictions of the $(\pm 30/90_4)_s$ and $(\pm 40/90_4)_s$ laminates (Figs. 5 and 6, resp.). For these two laminates, however, the onset of damage in the angle plies already occurs at lower strains and with slightly more effect on the predicted modulus degradation.

The analyses using in-situ strengths do not predict any cracking of the outer layers for the first two laminates within the strain interval considered. For laminates $(\pm 30/90_4)_s$ and $(\pm 40/90_4)_s$, the Poisson's ratio curves show two kinks which correspond to damage onset in the $+\beta$ and the $-\beta$ plies, respec-

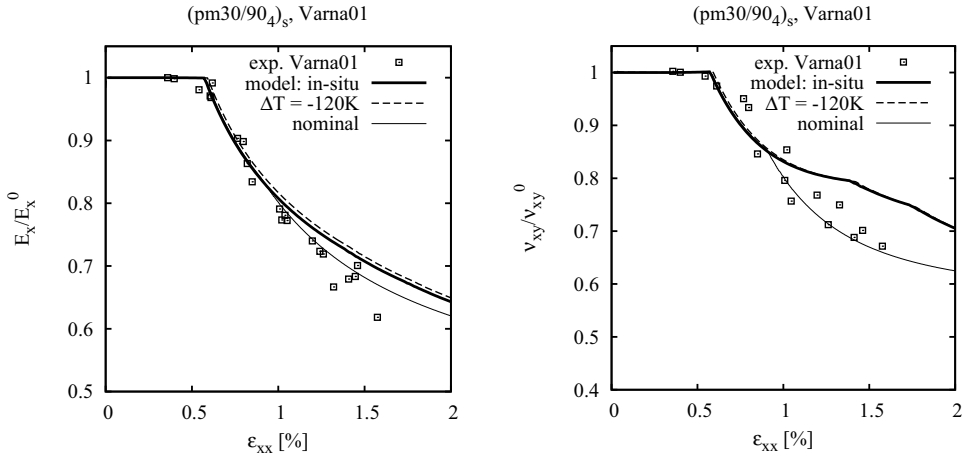

Fig. 5. Results for lay-up $(\pm 30/90_4)_s$; axial modulus (left) and laminate Poisson's ratio (right) normalized by their initial value; experimental data from [32].

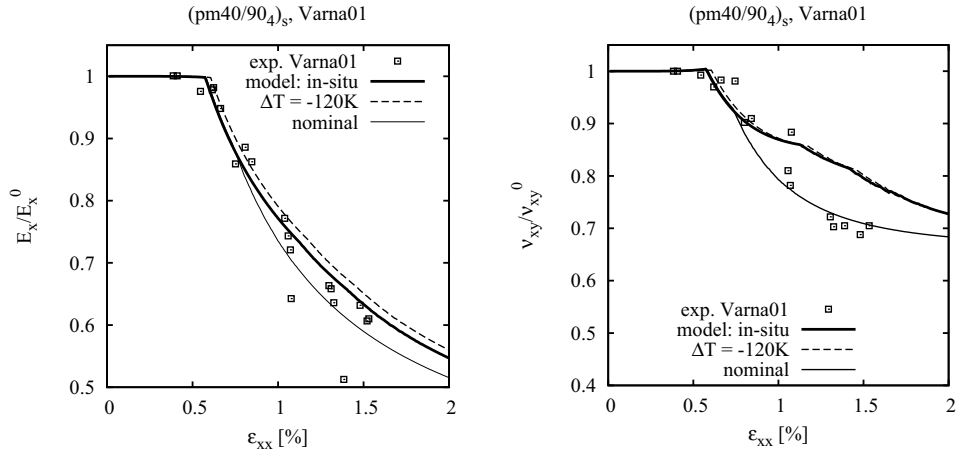

Fig. 6. Results for lay-up $(\pm 40/90_4)_s$; axial modulus (left) and laminate Poisson's ratio (right) normalized by their initial value; experimental data from [32].

Table 3
Nominal and in-situ strength values used in the analyses.

	in-situ					nominal
ply thickness	$t = t^{\text{ply}}$		$t = 2\,t^{\text{ply}}$	$t = 4\,t^{\text{ply}}$	$t = 8\,t^{\text{ply}}$	all
ply location	inner	outer	outer	inner	inner	—
Y^{t} [MPa]	213	151	107	107	76	76
S [MPa]	101	91	82	82	73	73
in-situ, $\Delta T = -120\,\text{K}$						
Y^{t} [MPa]	241	170	120	120	85	
S [MPa]	104	95	85	85	76	

tively. The fact that $+\beta$ and $-\beta$ plies do not start to crack at the same time is a result of the different in-situ strengths of outer and inner plies according to Eqs. 10 and 11. For all four lay-ups, there is little difference between the predictions with and without residual stresses.

It is interesting to note that the 'nominal' predictions, in general, show better correlation to experiments than the ones that include the in-situ effect. It should be kept in mind, however, that damage onset in the angle plies depends very much on shear strength, especially for high values of lay-up angle β, and that the shear strength is an estimated value. Regarding the in-situ predictions, there are two additional aspects that lead to further uncertainty. First, there may be some interaction between damage evolution in neighboring layers due to local stress concentrations near cracks in adjacent plies that cannot be accounted for in a continuum damage approach. Second, the laminate becomes unsymmetrical when damage evolves differently in $+\beta$ and $-\beta$ plies. In that case, the loading of a test specimen is different from the assumed uniaxial loading. Taking all these aspects into consideration, it is difficult to draw any firm conclusions on the applicability of the in-situ strength predictions. However, judging from the model predictions, it is likely that cracking of the angle plies contributes to the measured degradation in Figs. 5 and 6.

3.3 Laminate tests $(0/\pm\beta_4/0_{1/2})_s$

The second series of tests reported in [31] was performed on laminates with a stacking sequence $(0/\pm\beta_4/0_{1/2})_{\text{s}}$ and five angles $\beta = 90°, 70°, 55°, 40°, 25°$. Non-linearity in these laminates originates only from the β-plies, which experience varying stress ratios, σ_{22}/σ_{12}, depending on the angle β. Since the experi-

mental data only provides laminate stresses and strains, ply stress states have to be computed via CLT and depend on the assumed constitutive response. The ply loading paths in $\sigma_{12} - \sigma_{22}$ stress space computed from the laminate strains are shown in Fig. 7. Loading paths assuming linear elastic plies are depicted as thick solid arrows. For lay-up angles $\beta = 90°, 70°$ and $55°$, the arrowheads indicate the stress states corresponding to the laminate strain at which cracking initiated in the experiments [31]. For $\beta = 40°$ and $\beta = 25°$, no cracking was observed during the tests, and the arrowheads indicate the start of non-linearity in the experiments.

According to the combined model, stress states with a small ratio of σ_{22}/σ_{12}, i.e. here for laminates with angles $\beta = 55°, 40°$ and $25°$, lead to significant plastic strain prior to damage onset. The ply stress states during loading predicted by the plasticity part of the model (i.e. suppressing the onset of damage) are shown by dashed lines in Fig. 7 and deviate significantly from the stress ratios computed for linear elastic plies as the amount of plasticity increases. The curve for $\beta = 55°$ is plotted up to $\varepsilon_{xx} = 1.134\%$ which represents the average damage onset strain in tests of that lay-up. For $\beta = 40°$ and $\beta = 25°$, the dashed curves terminate at $\varepsilon_{xx} = 2\%$ which constitutes the strain range tested without onset of cracking. In other words, the ply stress states given by the three dashed lines represent strain states that did not cause any cracking in the three corresponding experiments. For $\beta = 90°$ and $\beta = 70°$, the plasticity model does not predict any non-linearity and would therefore result in the same loading path as given by the black arrows.

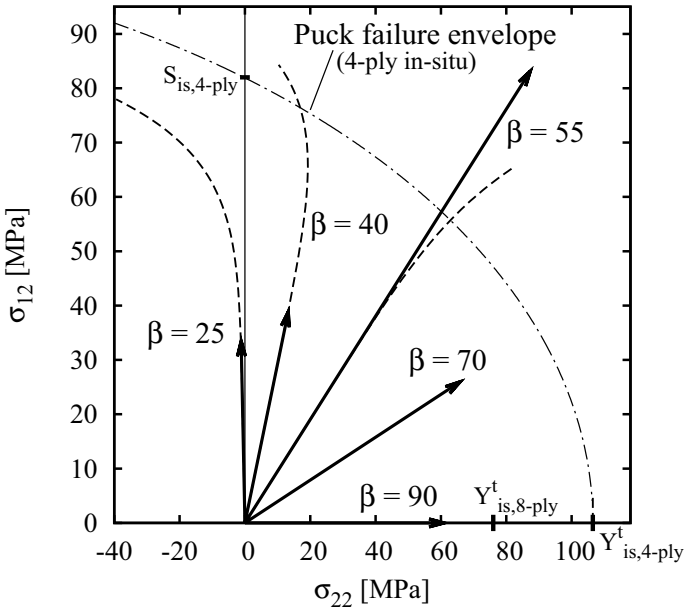

Fig. 7. Loading paths of β-plies in $(0/\pm\beta_4/0_{1/2})_s$ laminates subjected to uniaxial tension and theoretical ply failure stresses using in-situ strengths and Puck 2D failure criterion.

Also shown in Fig. 7 is the Puck failure envelope (using 4-ply in-situ strengths) which determines damage onset in the damage / plasticity model. For the special case of $\beta = 90$, the 8-ply in-situ strength, $Y_{\mathrm{is}}^{\mathrm{t}} = 76\,\mathrm{MPa}$, has to be applied. Comparing the stress states computed from the laminate strains at the onset of cracking to the Puck failure envelope reveals some discrepancies. In the $\beta = 90°$ and $\beta = 70°$ laminates, damage seems to develop prematurely, i.e. the arrows in Fig. 7 do not reach the theoretical failure stress. On the other hand, the predictions of the plasticity model for $\beta = 55°$ and $\beta = 40°$ suggest that, in these tests, the stress states at failure (ends of dashed lines) exceed the failure envelope. Since the value of $G_{\mathrm{IIc,ply}}$ (and therefore S_{is}) is only an estimate due to the lack of experimental data, the underprediction of damage onset for $\beta = 40°$ merely indicates that the actual shear strength is higher than the estimated one. For $\beta = 90°$, the deviation may be acceptable considering the typical scatter of experimental data. The discrepancy for $\beta = 70°$ and $\beta = 55°$, however, seems too high to be explained by scatter. Especially the fact that damage onset is overpredicted for $\beta = 70°$ but severely underpredicted for $\beta = 55°$ is surprising. Therefore, it has to be concluded that damage onset under multiaxial stress states is not yet completely understood and will require further investigation.

In Figs. 8–12, the degradation of axial modulus and laminate Poisson's ratio normalized by their respective initial values are shown for all five laminates. The experimental data points are taken from [31]. Note that the degradation curves for $\beta = 90°, 70°$, and $55°$ in [31] are given as a function of crack density, which can be converted to axial strain by the corresponding analytical expressions also provided in [31]. Model predictions are performed using in-situ strengths with and without residual stresses. For each of the cases $\beta = 70°, 55°$, and $40°$, a third analysis labeled 'best fit' is performed in which the strengths $Y_{\mathrm{is}}^{\mathrm{t}}$ and S_{is} are adjusted such that damage onset matches the experimental

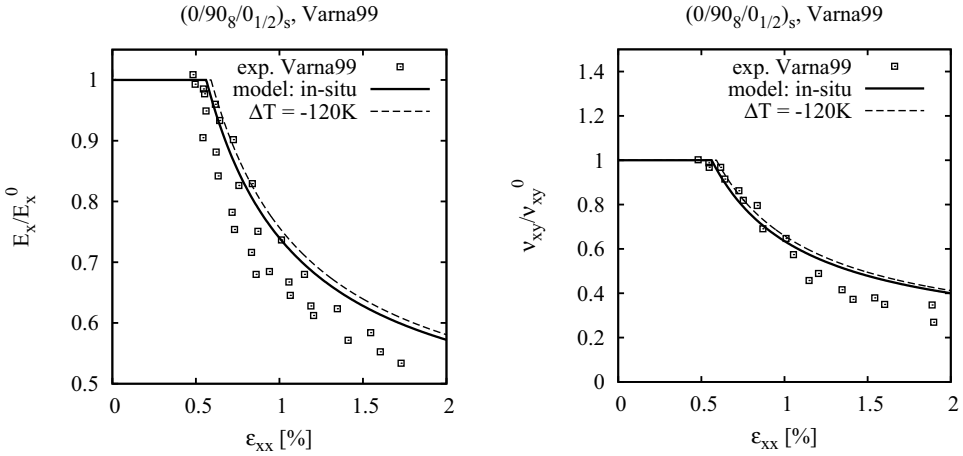

Fig. 8. Results for lay-up $(0/90_8/0_{1/2})_{\mathrm{s}}$; axial modulus (left) and laminate Poisson's ratio (right) normalized by their initial value; experimental data from [31].

data for each test case. This means that for those 'best fit' analyses, the failure envelope depicted in Fig. 7 is modified by changing $Y_{\mathrm{is}}^{\mathrm{t}}$ and S_{is} such that the envelope passes through the end point of the respective loading curve in Fig. 7 (i.e. the arrowhead for $\beta = 70°$ and the end points of the dashed lines for $\beta = 55°$, and $\beta = 40°$). The purpose of these adjustments is to see whether the degradation behavior is captured correctly when the uncertainty of ply strengths is factored out.

As can be seen in Figs. 8–12, the correlation between test results and model predictions is very good except for the discrepancy in damage onset discussed above. Similarly to the first series of tests in Section 3.2, there is only small difference between predictions with and without residual stresses. Also in analogy to observations in the previous section, it is found that the different ef-

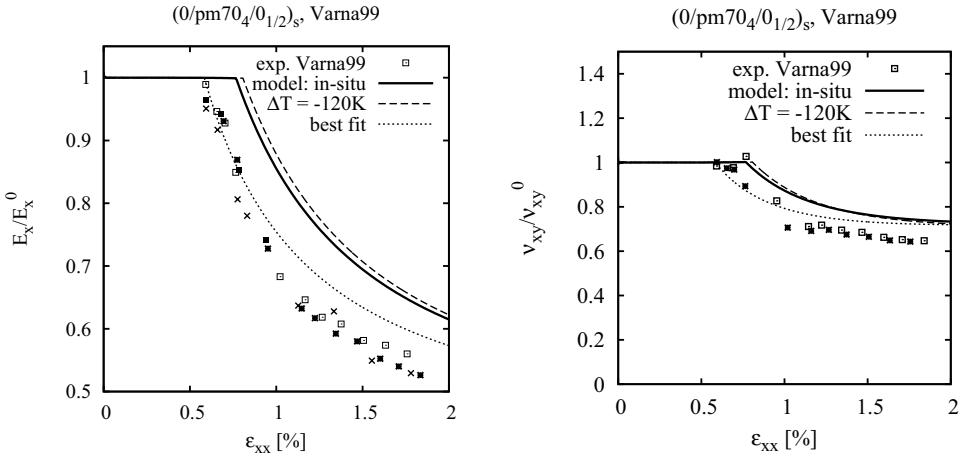

Fig. 9. Results for lay-up $(0/\pm 70_4/0_{1/2})_{\mathrm{s}}$; axial modulus (left) and laminate Poisson's ratio (right) normalized by their initial value; experimental data from [31].

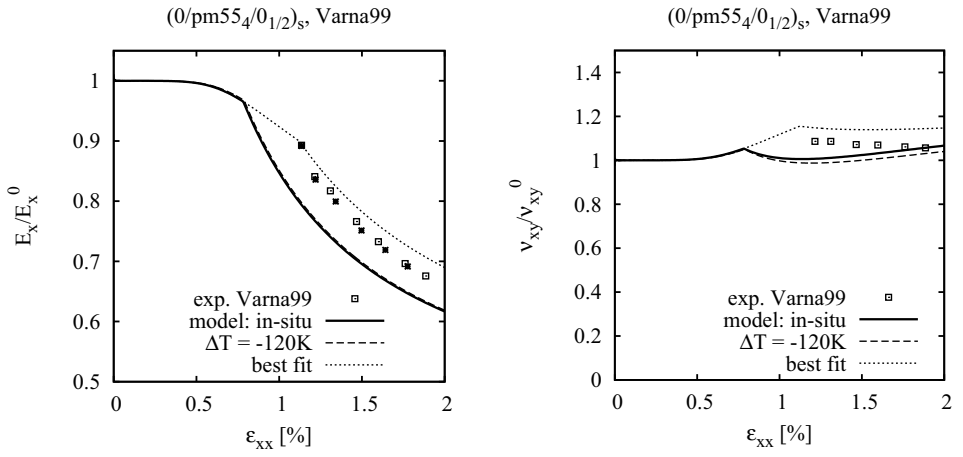

Fig. 10. Results for lay-up $(0/\pm 55_4/0_{1/2})_{\mathrm{s}}$; axial modulus (left) and laminate Poisson's ratio (right) normalized by their initial value; experimental data from [31].

fects contributing to non-linearity are much more apparent in the degradation curves of Poisson's ratio than those of axial modulus. The non-linearity for $\beta = 90°$ and $\beta = 70°$ is caused by damage only and leads to a decrease in axial modulus as well as in Poisson's ratio (Figs. 8 and 9). For $\beta = 40°$ and $\beta = 25°$, on the other hand, non-linearity is primarily due to plasticity which reduces the axial modulus but increases the laminate Poisson's ratio (Figs. 11 and 12). In the $\beta = 55°$ laminate, damage and plasticity both contribute to the non-linear response (Fig. 10). Consequently, the Poisson's ratio increases at first as a result of plasticity, but when damage and plastic strains accumulate simultaneously, the Poisson's ratio stays approximately constant, i.e. the opposing effects of damage and plasticity on Poisson's ratio cancel each other out.

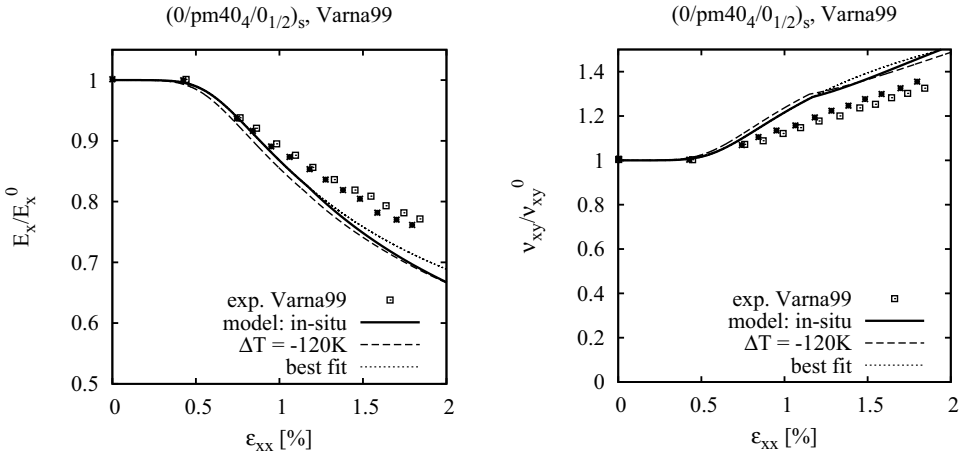

Fig. 11. Results for lay-up $(0/\pm 40_4/0_{1/2})_s$; axial modulus (left) and laminate Poisson's ratio (right) normalized by their initial value; experimental data from [31].

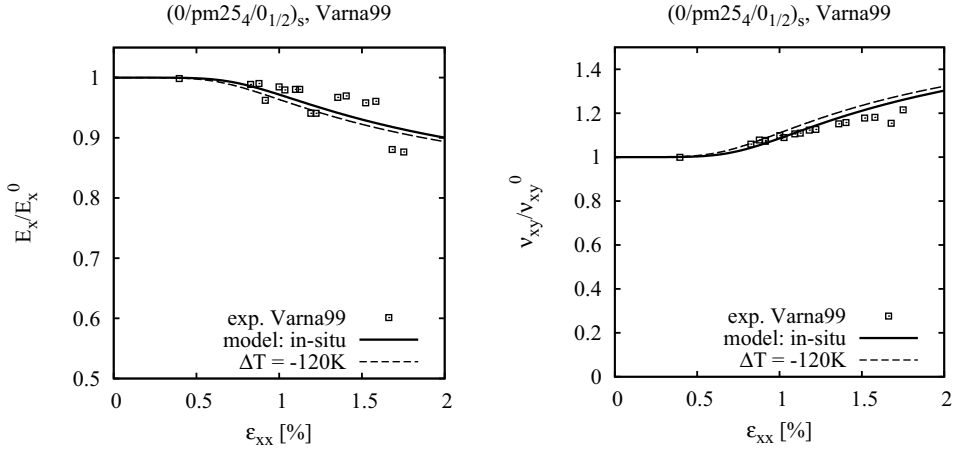

Fig. 12. Results for lay-up $(0/\pm 25_4/0_{1/2})_s$; axial modulus (left) and laminate Poisson's ratio (right) normalized by their initial value; experimental data from [31].

In general, stiffness degradation related to damage seems to be slightly underestimated by the model (see Figs. 8 and 9 as well as Section 3.2) while plastic strains tend to be slightly overpredicted. However, the overall correlation with experimental data regarding non-linearity is satisfactory and the different effects of damage and plasticity on the non-linear response are captured very well by the combined damage / plasticity model. The main issue that requires further investigation is the discrepancy between model and experiments regarding damage onset under multi-axial stress states.

4 CONCLUSIONS

A ply-level model for fiber reinforced composites is proposed that combines plasticity and continuum damage mechanics to predict the non-linear response of polymer composite laminates. The Puck criterion for plane stress states is used for predicting damage onset in the model. To account for the in-situ effect in thin embedded plies, an analytical fracture mechanics based solution is adopted to compute in-situ strengths as a function of ply thickness.

The proposed model is used to predict the load response of various laminates under uniaxial tension, and results are compared to experimental data from two series of tests from the literature. Parameters for the plasticity formulation of the model are identified from test data independent from the test data used in the comparisons. The damage parameters that control stiffness degradation due to damage are chosen as typical values for glass fiber materials.

The first series of tests consists of a thick 90° layer embedded in various angle-ply sublaminates. While most of the non-linearity in these laminates is due to damage in the 90° plies, it is demonstrated by the analyses that in some cases damage in the sublaminates is likely to contribute to the non-linearity. The second test series investigates non-linearity due to multi-axial ply stress states by using laminates consisting of angle-ply sublaminates embedded between 0° layers. The main challenge in these tests is found to be the prediction of damage onset for various stress ratios σ_{22}/σ_{12}. Apart from the unresolved problem of damage onset, the different effects of plasticity and damage on the non-linear response are captured very well by the proposed model.

The influence of residual stresses on predictions for both test series is investigated. It is found that residual stresses have little effect on the results, which is partly due to the fact that ply strengths are determined from the onset of cracking in an embedded layer. Therefore, residual stresses are implicitly taken into account to a certain extent even when they are not modeled directly. When ply strengths are determined from UD laminate tests, it is to be expected that residual stresses have a significant influence on damage onset.

An interesting observation made from the comparison to experiments is that the degradation of Poisson's ratio can give valuable additional information. For example, the additional degradation due to successive damage onset in several layers predicted for test cases of the first test series, is much more apparent in the degradation of Poisson's ratio than in that of axial modulus. Furthermore, in the second series of tests, the Poisson's ratio degradation clearly shows that there are two different mechanisms responsible for the non-linear response. One mechanism leads to an increase of Poisson's ratio while the other mechanism causes a decrease. In the present model the two mechanisms are interpreted as matrix plasticity and matrix cracking. Since both mechanisms result in a reduction of the axial modulus, the two mechanisms cannot be distinguished by looking at the degradation of axial modulus only.

Acknowledgement

This research was supported by the NASA Postdoctoral Program at NASA Langley Research Center, administered by Oak Ridge Associated Universities. The funding of the Austrian Aeronautics Research (AAR) / Network for Materials and Engineering by the Austrian Federal Ministry of Economics and Labor is gratefully acknowledged.

REFERENCES

[1] D. H. Allen. Damage evolution in laminates. In R. Talreja, editor, *Damage Mechanics of Composite Materials*, volume 9 of *Composite Materials Series*, chapter 3. Elsevier Science Ltd., Oxford, UK, 1994.

[2] O. Allix, L. Daudeville, and P. Ladevèze. Delamination and damage mechanics. In D. Baptiste, editor, *Mechanics and Mechanisms of Damage in Composites and Multi-Materials*, pages 143–158. Mechanical Engineering Publications Limited, London, UK, 1991.

[3] D. Aragonés. Fracture micromechanisms in C/epoxy composites under transverse compression. Master's thesis, Universidad Politécnica de Madrid, 2007.

[4] E. J. Barbero and P. Lonetti. An inelastic damage model for fiber reinforced laminates. *J. Comp. Mat.*, 36(8):941–962, 2002.

[5] B. A. Bednarcyk. A fully coupled micro/macro theory for thermo-electro-magneto-elasto-plastic composite laminates. Technical Report CR—2002-211468, NASA, 2002.

[6] P. P. Camanho, C. G. Dávila, S. T. Pinho, L. Iannucci, and P. Robinson. Prediction of in situ strengths and matrix cracking in composites under transverse tension and in-plane shear. *Composites Part A*, 37(2):165–176, 2006.

[7] P. P. Camanho, J. A. Mayugo, P. Maimí, and C. G. Dávila. A micromechanics-based damage model for the strength prediction of composite laminates. In *Proc. of European Conference on Computational Mechanics (ECCM 2006), June 5–9, 2006, Lisbon, Portugal*. Paper 1661, 2006.

[8] F. W. Crossman, W. J. Warren, A. S. D. Wang, and G. E. Law Jr. Initiation and growth of transverse cracks and edge delamination in composite laminates, part 2: Experimental results. *J. Comp. Mat.*, 14:88–108, 1980.

[9] H. T. Hahn and S. W. Tsai. Nonlinear elastic behaviour of unidirectional composite laminates. *J. Comp. Mat.*, 7:102–110, 1973.

[10] R. Joffe and J. Varna. Analytical modeling of stiffness reduction in symmetric and balanced laminates due to cracks in 90° layers. *Comp. Sci. and Tech.*, 59:1641–1652, 1999.

[11] P. Ladevèze. On a damage mechanics approach. In D. Baptiste, editor, *Mechanics and Mechanisms of Damage in Composites and Multi-Materials*, pages 119–142. Mechanical Engineering Publications Limited, London, UK, 1991.

[12] J. Lemaitre. *A Course on Damage Mechanics*. Springer Verlag, Berlin Heidelberg, Germany, 1992.

[13] T. Mori and K. Tanaka. Average stress in the matrix and average elastic energy of materials with misfitting inclusions. *Acta Metall.*, 21:571–574, 1973.

[14] J. A. Nairn and S. Hu. Matrix microcracking. In R. Talreja, editor, *Damage Mechanics of Composite Materials*, volume 9 of *Composite Materials Series*, chapter 6. Elsevier Science Ltd., Oxford, UK, 1994.

[15] A. Parvizi, K. Garrett, and J. Bailey. Constrained cracking in glass fiber reinforced epoxy cross-ply laminates. *J. Mat. Sci.*, 13:195–201, 1978.

[16] K. Pettersson. *The Inclined Double Notch Shear Test for Determination of Interlaminar Shear Properties of Composite Laminates*. PhD thesis, Royal Institute of Technology, Solid Mechanics, Stockholm, Sweden, 2005.

[17] A. Puck. *Festigkeitsanalyse von Faser-Matrix-Laminaten*. Carl Hanser Verlag, München Wien, Germany, 1996.

[18] A. Puck, J. Kopp, and M. Knops. Guidelines for the determination of the parameters in Puck's action plane strength criterion. *Comp. Sci. and Tech.*, 62:(3) 371–378; (9) 1275, 2002.

[19] A. Puck and M. Mannigel. Physically based non-linear stress–strain relations for the inter-fibre fracture analysis of FRP laminates. *Comp. Sci. and Tech.*, 67:1955–1964, 2007.

[20] A. Puck and H. Schürmann. Failure analysis of FRP laminates by means of physically based phenomenological models. *Comp. Sci. and Tech.*, 58:1045–1067, 1998.

[21] J. N. Rabotnov. *Creep Problems in Structural Members*, volume 7 of *North-Holland series in Applied Mathematics and Mechanics*. North-Holland, Amsterdam, Netherlands, 1969.

[22] C. Schuecker. *Mechanism based modeling of damage and failure in fiber reinforced polymer laminates*. PhD thesis, Institute of Lightweight Design and Structural Biomechanics, Vienna University of Technology, Vienna, Austria, 2005. (also published in: VDI Fortschritt-Berichte VDI Reihe 18 Nr. 303. VDI-Verlag, Düsseldorf).

[23] C. Schuecker, D. H. Pahr, and H. E. Pettermann. Accounting for residual stresses in FEM analyses of laminated structures using the Puck criterion for three-axial stress states. *Comp. Sci. and Tech.*, 66(13):2054–2062, 2006.

[24] C. Schuecker and H. E. Pettermann. A continuum damage model for fiber reinforced laminates based on ply failure mechanisms. *Composite Structures*, 76(1-2):162–173, 2006.

[25] C. Schuecker and H. E. Pettermann. Combining progressive damage with plasticity to model the non-linear behavior of fiber reinforced laminates. In *Proc. of the ECCOMAS Thematic Conference: Mechanical Response of Composites, Sept. 12–14, 2007, Porto, Portugal*. Paper p41, 2007. (Extended version to appear in *Mechanical Response of Composites*, ECCOMAS book series, Springer).

[26] C. Schuecker and H. E. Pettermann. Constitutive ply damage modeling, FEM implementation, and analyses of laminated structures. *Comput. and Struct.*, 86(908-918), 2008.

[27] I. Shahid and F.K. Chang. An accumulative damage model for tensile and shear failures of laminated composite plates. *J. Comp. Mat.*, 29(7):926–981, 1995.

[28] R. Talreja, S. Yalvac, L. D. Yats, and D. G. Wetters. Transverse cracking and stiffness reduction in cross ply laminates of different matrix toughness. *J. Comp. Mat.*, 26(11):1644–63, 1992.

[29] G. P. Tandon and G. J. Weng. The effect of aspect ratio of inclusions on the elastic properties of unidirectionally aligned composites. *Polym. Compos.*, 5:327–333, 1984.

[30] W. Van Paepegem, I. De Baere, and J. Degrieck. Modelling the nonlinear shear stress–strain response of glass fibre-reinfroced composites. Part I: Experimental results. *Comp. Sci. and Tech.*, 66(10):1455–1464, 2006.

[31] J. Varna, R. Joffe, N. V. Akshantala, and R. Talreja. Damage in composite laminates with off-axis plies. *Comp. Sci. and Tech.*, 59:2139–2147, 1999.

[32] J. Varna, R. Joffe, and R. Talreja. A synergistic damage-mechanics analysis of transverse cracking in $[\pm\theta/90_4]_s$ laminates. *Comp. Sci. and Tech.*, 61:657–665, 2001.

REPORT DOCUMENTATION PAGE

Form Approved
OMB No. 0704-0188

1. REPORT DATE *(DD-MM-YYYY)*	2. REPORT TYPE	3. DATES COVERED *(From - To)*
01- 07 - 2008	Technical Memorandum	

4. TITLE AND SUBTITLE

Modeling the Non-Linear Response of Fiber-Reinforced Laminates Using a Combined Damage/Plasticity Model

5a. CONTRACT NUMBER

5b. GRANT NUMBER

5c. PROGRAM ELEMENT NUMBER

6. AUTHOR(S)

Schuecker, Clara; Dávila, Carlos G.; and Pettermann, Heinz E.

5d. PROJECT NUMBER

5e. TASK NUMBER

5f. WORK UNIT NUMBER

698259.02.07.07.03.03

7. PERFORMING ORGANIZATION NAME(S) AND ADDRESS(ES)

NASA Langley Research Center
Hampton, VA 23681-2199

8. PERFORMING ORGANIZATION REPORT NUMBER

L-19487

9. SPONSORING/MONITORING AGENCY NAME(S) AND ADDRESS(ES)

National Aeronautics and Space Administration
Washington, DC 20546-0001

10. SPONSOR/MONITOR'S ACRONYM(S)

NASA

11. SPONSOR/MONITOR'S REPORT NUMBER(S)

NASA/TM-2008-215314

12. DISTRIBUTION/AVAILABILITY STATEMENT

Unclassified - Unlimited
Subject Category 24
Availability: NASA CASI (301) 621-0390

13. SUPPLEMENTARY NOTES

An electronic version can be found at http://ntrs.nasa.gov

14. ABSTRACT

The present work is concerned with modeling the non-linear response of fiber reinforced polymer laminates. Recent experimental data suggests that the non-linearity is not only caused by matrix cracking but also by matrix plasticity due to shear stresses. To capture the effects of those two mechanisms, a model combining a plasticity formulation with continuum damage has been developed to simulate the non-linear response of laminates under plane stress states. The model is used to compare the predicted behavior of various laminate lay-ups to experimental data from the literature by looking at the degradation of axial modulus and Poisson's ratio of the laminates. The influence of residual curing stresses and in-situ effect on the predicted response is also investigated. It is shown that predictions of the combined damage / plasticity model, in general, correlate well with the experimental data. The test data shows that there are two different mechanisms that can have opposite effects on the degradation of the laminate Poisson's ratio which is captured correctly by the damage / plasticity model. Residual curing stresses are found to have a minor influence on the predicted response for the cases considered here. Some open questions remain regarding the prediction of damage onset.

15. SUBJECT TERMS

Non-linear material response; Plasticity; Polymer matrix composites; Puck failure criteria

16. SECURITY CLASSIFICATION OF:			17. LIMITATION OF ABSTRACT	18. NUMBER OF PAGES	19a. NAME OF RESPONSIBLE PERSON
a. REPORT	b. ABSTRACT	c. THIS PAGE			STI Help Desk (email: help@sti.nasa.gov)
					19b. TELEPHONE NUMBER *(Include area code)*
U	U	U	UU	29	(301) 621-0390